Dalton Transactions



COMMUNICATION

View Article Online
View Journal | View Issue



Cite this: *Dalton Trans.*, 2025, **54**, 12130

Received 15th May 2025, Accepted 11th July 2025 DOI: 10.1039/d5dt01140j

rsc.li/dalton

Structural control of μ -hydroxo- μ -peroxodicobalt(III) complex with the 6-hpa dinucleating ligand to enhance O_2 -evolution activity in catalytic water oxidation†

Yuki Tanaka,^a Osamu Iwanaga,^a Kyosuke Fujikawa,^a Seina Shinomiya,^a Hiroaki Kitagishi, ^b ^a Sachiko Yanagisawa,^b Minoru Kubo,^b Tetsuya Kambe, ^b ^c Shigenobu Masaoka ^c ^a and Masahito Kodera ^b *

The 6-hpa ligand forms a μ -hydroxo- μ -peroxodicobalt(III) complex [Co(μ -OH)(μ -O₂)(6-hpa)]X₃ (X = ClO₄ (1a) and PF₆ (1b)) and controls the formation of syn configuration. Electrochemical studies revealed that the 6-hpa ligand lowers the oxidation potential of the peroxide moiety by 0.13 V and twice enhances O₂ evolution during catalytic water oxidation by fixing the syn configuration.

The development of sustainable systems is attracting great social attention, given the mounting global warming and energy problems. Oxygen evolution by the O_2 -evolving complex (OEC), a Mn_4CaO_5 cluster, during photosynthesis in plant cells is a key reaction essential for sustainable systems. In 1982, Meyer reported a diruthenium complex, so-called the blue dimer, as the first artificial water oxidation catalyst. Recently, various cheap and abundant metals such as Mn_5 Fe, and Co^7 have been used instead of expensive and rare Ru for water oxidation catalysts.

Thapper reported that the μ -hydroxo- μ -peroxodicobalt(III) complex with the tpa ligand (tris(2-pyridylmethyl)amine) [Co (μ -OH)(μ -O₂)(tpa)₂](ClO₄)₃ (2) catalyses O₂ evolution *via* water oxidation in a photochemical reaction.⁸ Lue claimed that 2 decomposes to give CoO_x nanoparticles, deposited on the electrode in the electrolytic reaction, to catalyze the reaction as heterogeneous catalysts.⁹ Kojima reported that 2-syn and 2-anti, diastereomers of 2, show different O₂-evolving activity.¹⁰

We have reported diiron¹¹ and dicopper¹² complexes with the 6-hpa ligand (1,2-bis{2-[bis(2-pyridylmethyl)aminomethyl]-

The ClO_4 salt **1a** was obtained as dark-blue crystals upon reaction of 6-hpa ligand with $Co(ClO_4)_2 \cdot 6H_2O$ in the presence of Et_3N in MeOH under O_2 ; the crystals were used for the spectroscopic and electrochemical studies. The PF_6 salt **1b** was prepared for the structure analysis. The synthetic details of **1a** and **1b** are shown in the $ESI.\dagger$

The peroxodicobalt(III) complexes **1b**, **2-syn**, and **2-anti** were structurally characterized by X-ray analysis (Fig. S1:† ORTEP views of **2-syn** and **2-anti**; Table S1:† the crystallographic data; and Tables S2, S3, and S4:† selected bond distances and

[†]Electronic supplementary information (ESI) available: Detailed experimental procedures, Fig. S1–S5, Tables S1–S6. CCDC 2415276. For ESI and crystallographic data in CIF or other electronic format see DOI: https://doi.org/10.1039/d5dt01140j

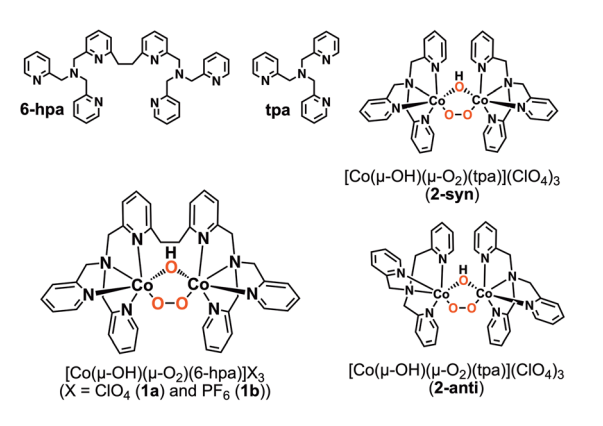


Fig. 1 Chemical structures of ligands and Co complexes.

⁶⁻pyridyl}-ethane), where a $-CH_2CH_2-$ tether connects two tpa units. The chemical structures of tpa and 6-hpa are shown in Fig. 1. The 6-hpa ligand enabled the conversion between peroxodiiron(III) and dioxodiiron(IV) species *via* reversible O–O bond scission and formation, where the 6-hpa ligand stabilizes these two species.¹³ In this study, we report the synthesis, structure, and catalytic water oxidation of μ-hydroxo-μ-peroxodicobalt(III) complexes with 6-hpa $[Co(μ-OH)(μ-O_2)(6-hpa)]X_3$ (X = ClO_4 (1a) and PF_6 (1b)) and the effect of 6-hpa ligand fixing the *syn* configuration on the O–O bond formation in catalytic water oxidation.

^aDepartment of Molecular Chemistry and Biochemistry, Doshisha University, Kyotanabe, Kyoto 610-0321, Japan. E-mail: mkodera@mail.doshisha.ac.jp ^bGraduate School of Science, University of Hyogo, 3-2-1 Kouto, Kamigori, Ako, Hyogo 678-1297, Japan

^cDivision of Applied Chemistry, Graduate School of Engineering, Osaka University, 2-1 Yamadaoka, Suita, Osaka 565-0871, Japan

Dalton Transactions Communication

angles of 1b, 2-syn, and 2-anti; ESI†). The ORTEP view of 1b is shown in Fig. 2. The 6-hpa ligand encapsulates a μ-OH-μ-O₂-Co $(III)_2$ core to take the syn configuration, where the $-CH_2CH_2$ tether makes anti configuration impossible. This is the structural control by the 6-hpa ligand. Compound 1b is structurally similar to the syn configuration of 2-syn but not to the anti configuration of 2-anti. The Co···Co and O-O bond distances of 3.254 and 1.395 Å in 1b are close to the 3.255 and 1.383 Å in **2-syn** and longer than the 3.246 and 1.356 Å in **2-anti**. The Co-O-O-Co dihedral angle 53.4(3)° in 1b is far smaller than the $61.2(4)^{\circ}$ and $63.4(4)^{\circ}$ in 2-syn and 2-anti. Thus, the dicobalt core of **1b** is more planar than those of **2-syn** and **2-anti**. ¹⁶ The average Co-O_{peroxide} bond distance of 1.842 Å in 1b is slightly shorter than the 1.851 Å and 1.865 Å in 2-syn and 2anti. 15 The short Co-Operoxide bond and planar core structure makes the $d\pi$ -p π interactions of Co-O_{peroxide} bonds stronger in

The structure of the 6-hpa complex 1a in solution was spectroscopically examined. The ¹H NMR spectra of 1a and of a mixture of 2-syn and 2-anti, measured in a deuterated Britton-Robinson (B-R) buffer, 14 are shown in Fig. S2 and S3 (ESI)† along with the peak assignments in Tables S5 and S6 (ESI),† respectively. The ¹H NMR signals of 2-syn and 2-anti were assigned according to the literature. 10 In the chemical shifts of 6-H atoms in equatorial py groups, the 9.48 ppm red color a in 2-syn is higher than the 9.40 and 9.27 ppm purple color a and a' in 2-anti (Fig. S3 and Table S6, ESI†), and the 9.48 and 9.40 ppm of 6-H atoms close to μ-O₂ are higher than the 9.27 ppm of that close to μ-OH. The integral ratio (a in 2syn): (a in 2-anti): (a' in 2-anti) = 2:1.4:1.4. Since 2-syn has two equivalent 6-H atoms, the ratio of 2-syn: 2-anti is 1:1.4. The assymmetric unit in the ¹H NMR spectrum of 1a (Fig. S2, ESI†) is half of a molecular structure because 1a takes only syn configuration. Two equivalent equatorial py groups in 1a give four signals: a, c, d, and f. The two types among the four axial py groups of 1a are the pendant py groups and py groups connected by a -CH₂CH₂- tether, giving four signals (b, e, g, h) for the former and two signals (i, j) for the latter (Fig. S2 and

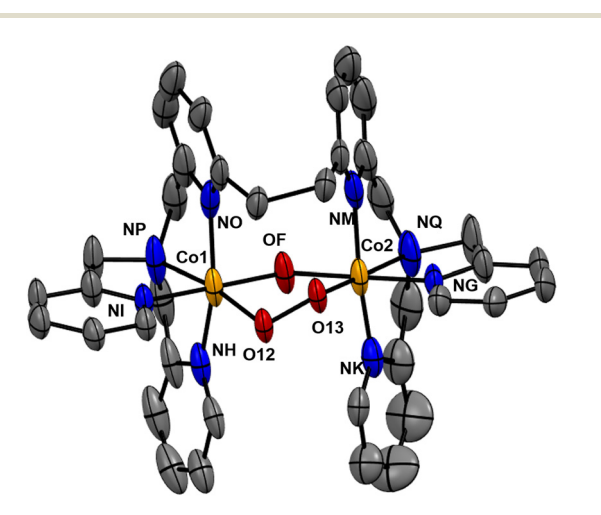


Fig. 2 ORTEP diagram of 1b. H-atoms are omitted for clarity.

Table S5, ESI†). The integration ratios are (a, c, d, f): (b, e, g, h) = 1:1 and i:j=2:1. The chemical shift of 9.87 ppm for the 6-H of the equatorial py group in 1a is much higher than the 9.48 ppm in 2-syn because the syn configuration of 1a is tightly fixed by the 6-hpa ligand.

Resonance Raman spectra of 1a and the mixture of 2-syn and 2-anti in MeCN at -30 °C are shown in Fig. 3(A) and (B), respectively. Compound 1a gave a single O-O stretching vibration band, and the mixture of 2-syn and 2-anti gave two bands. These are consistent with the crystal structures and ¹H NMR spectra showing that the 6-hpa ligand forms only the syn form, and for the tpa ligand, both the syn and anti forms. Since the ratio of 2-syn and 2-anti is 1:1.4, as shown by the ¹H NMR spectrum, the $\nu_{160-160}$ band at 845 cm⁻¹ of slightly weaker intensity is assigned to 2-syn, and that at 866 cm⁻¹ to **2-anti.** These are close to the $\nu_{16\mathrm{O}-16\mathrm{O}}$ bands 844 and 874 cm⁻¹ reported for 2-syn and 2-anti. The $\nu_{180-180}$ bands of 2-syn and 2-anti prepared under $^{18}O_2$ appeared at 794 and 816 cm $^{-1}$, and the isotope shifts are 51 and 50 cm⁻¹, respectively. Compound 1a showed the $\nu_{16O-16O}$ band at 867 cm⁻¹ and the $\nu_{180-180}$ band at 820 cm⁻¹. The isotope shift is 47 cm⁻¹. This value is close to 49.6 cm⁻¹, the theoretically calculated isotope shift for **1a** shown in ESI.† The $\nu_{16O-16O}$ band 867 cm⁻¹ of **1a** is higher by 22 cm⁻¹ than the 845 cm⁻¹ of 2-syn, indicating that the O-O bond of 1a is strengthened by the 6-hpa ligand encapsulating the μ -OH- μ -O₂-Co(III)₂ core.

The electrochemical properties of 1a and the mixture of 2syn and 2-anti were compared in the cyclic voltammograms (CV) and square wave voltammograms (SWV) measured in B-R buffer under N₂. In the CV at pH 8.0 (Fig. S4, ESI†), 1a shows a large oxidation wave at the onset potential of 1.2 V vs. NHE, with small reduction and oxidation waves at 0.6 and 1.0 V vs. NHE, but 2-syn and 2-anti showed a relatively small oxidation wave at the onset potential of 1.2 V vs. NHE, with unclear redox waves in the low-potential region. In the SWV at pH 8.0 (Fig. 4), 1a and the mixture of 2-syn and 2-anti show two redox

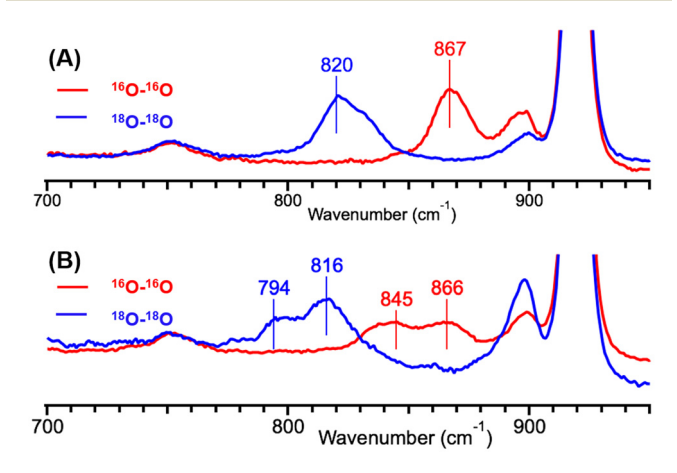


Fig. 3 Resonance Raman spectra of 1a (A) and a mixture of 2-syn and 2-anti (B) in MeCN at -30 °C with excitation at 405 nm. The spectra of $^{16}O-^{16}O$ and $^{18}O-^{18}O$ complexes are shown as red and blue lines, respectively.

Communication Dalton Transactions

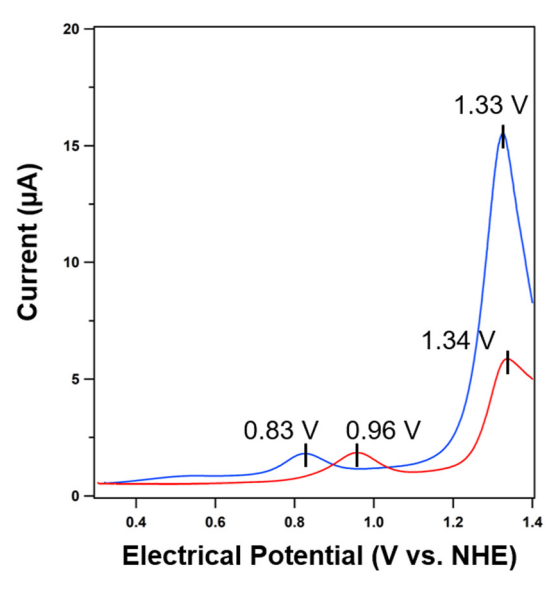


Fig. 4 SWV traces of 1a (blue) and the mixture of 2-syn and 2-anti (red) (0.1 mM) in B–R buffer at pH 8.0 at 298 K, using a 3 mm GC working electrode (0.07 cm 2), Pt wire counter electrode, Ag/AgCl reference electrode, potential increase: 0.001 V, amplitude: 0.025 A, frequency: 10 Hz, and sensitivity: 10 mAV $^{-1}$.

peaks at 0.83 and 1.32 V for **1a** and at 0.96 and 1.34 V for the mixture. The low-potential peak is assigned to the oxidation of peroxide moiety, and the high-potential peak to catalytic water oxidation. The low-potential peak at 0.83 of **1a** is lower by 0.13 V than the 0.96 V of **2-syn** and **2-anti**. This is because the $d\pi$ - $p\pi$ interaction in the Co-O_{peroxide} bond of **1a** is stronger than those of **2-syn** and **2-anti**. The strong $d\pi$ - $p\pi$ interaction increases the energy level of the anti-bonding orbital of the peroxide O atom to lower the oxidation potential. The catalytic current of water oxidation by **1a** is 2.7-fold higher than that by the tpa complexes. This shows that the 6-hpa ligand enhances the catalytic activity in the water oxidation of **1a** by fixing the *syn* form.

Fig. 5 shows the Pourbaix diagram of 1a and the mixture of 2-syn and 2-anti based on the SWV data (Fig. S5, ESI†) measured in a pH 3.0-8.0 range. The first redox peak of 1a is 0.95 V vs. NHE in the pH 3.0-5.5 region and shifts negatively from 0.94 to 0.83 V with a slope of 44 mV per pH in the pH 5.5-8.0 region. The second peak of 1a shifts negatively with a slope of 40 mV per pH from 1.45 to 1.39 V in the pH 4.0-5.5 region and is the same potential of zero slope in the pH 5.5-6.5 region. These slopes are almost the same as the 45 mV per pH reported for 2-syn and 2-anti. 10 The first and second peaks are assigned to oxidations of the peroxide moiety to form superoxo species and Co(III) to Co(IV), as reported for 2syn and 2-anti. 10 The redox potential of the peroxide moiety of 1a is lower by 0.13-0.15 V than those of 2-syn and 2-anti, but that of Co(III) to Co(IV) is slightly higher in 1a than in 2-syn and **2-anti.** Thus, the $d\pi$ -p π interaction is strengthened by the 6-hpa ligand, which facilitates the oxidation of peroxide moiety and slightly raises the redox potential of Co(III) to Co

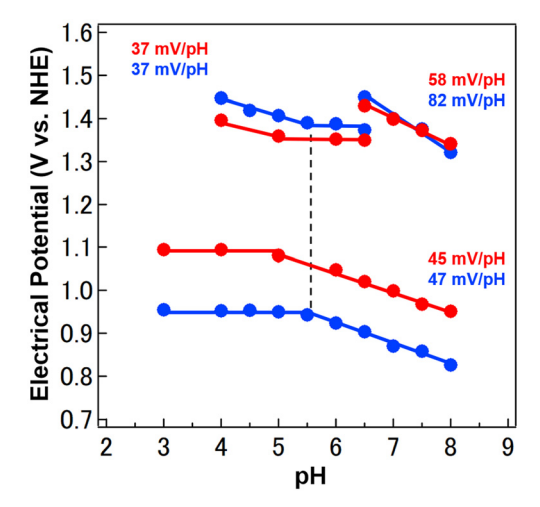


Fig. 5 Plots of redox potentials vs. pH values (Pourbaix diagram) for 1a (blue) and the mixture of 2-syn and 2-anti (red) in B-R buffer at 298 K. The mV per pH values are shown.

(rv). The third peak of **1a** shifted negatively, with a slope of 87 mV per pH from 1.45 to 1.32 V, in the pH 6.5–8.0 region and gave a large catalytic current in the water oxidation. This is much larger than the 27.5 mV per pH reported for the $2e^-$ oxidation and $1H^+$ release process in water oxidation by a $[Co^{III}(\mu\text{-OH})tpa]_2$ complex.¹⁰ The large slope indicates that $2e^-/H^+$ or $4e^-/2H^+$ PCET is involved as a key reaction in the catalytic water oxidation by **1a**.

Controlled potential electrolyses (CPE) of 1a and the mixture of 2-syn and 2-anti were performed at 1.4 V (vs. NHE) in B–R buffer at pH 6.0, 7.0, and 8.0. The O_2 generated during electrolysis was determined by GC analysis. Fig. 6 shows a plot of the turnover number (TON = moles of O_2 generated/moles of complex used) vs. reaction time. The time courses of O_2 evolution are composed of two parts, a first rapid reaction and the next slow one. The TON of O_2 evolution at the beginning of 3 h increased with increasing pH, showing that PCET is a key reaction in the catalytic water oxidation. Therefore, the first

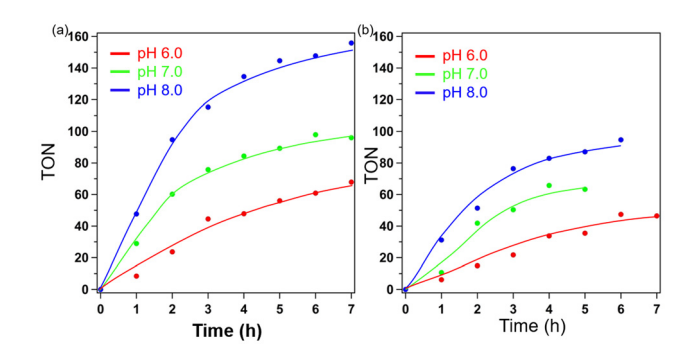


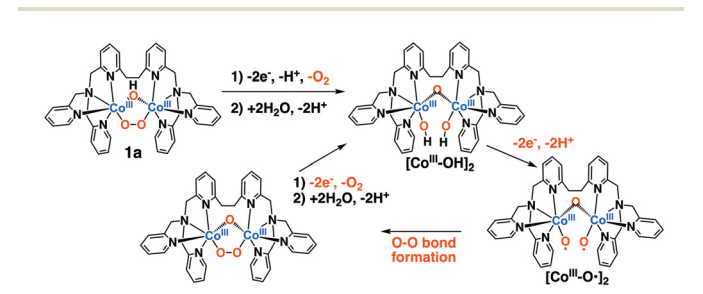
Fig. 6 The controlled potential electrolysis of 1a (a) and a mixture of 2-syn and 2-anti (b) (0.1 mM) was carried out at 1.4 V (vs. NHE) in B-R buffer at pH 6.0, 7.0, and 8.0. Conditions: working electrode Pt mesh, counter electrode Pt wire, reference electrode Ag/AgCl. The amount of O_2 evolution in the CPE was determined by GC analysis.

Dalton Transactions Communication

rapid O₂ evolution is catalysed by the Co complex. However, the O₂ evolution after 3 h did not depend on the pH and kind of Co complex used. This is totally different from the O2 evolution by Co complexes. The slow O2 evolution may be catalysed by CoO_x generated in the electrolytic reaction, as reported by Lue et al. (Fig. S8 and S9† for CoO_x formation). Thus, the reactions in the beginning of 3 h are used to compare the O2 evolution activity of the Co complexes. The O2 evolution by 1a is two-fold higher than that by a mixture of 2-syn and 2-anti. This is consistent with the 2.7-fold larger current of 1a than those of 2-syn and 2-anti observed in the SWV at 1.3 V. These results show that the syn configuration, fixed the by 6-hpa ligand, is a key feature enhancing O2 evolution in water oxidation by the 6-hpa Co complex. The UV-vis spectral change and current plot in the electrolytic water oxidation of 1a (Fig. S7†) showed that the LMCT band of 1a at 384 nm (Fig. S6†) rapidly decreased by the oxidation of peroxide moiety, where a superoxo species A, having absorption at 311 nm, was formed transiently and converted to an intermediate B having absorption at 271 nm kept in the steady-state O2 evolution.

The mechanism of the O2 evolution by 1a is proposed based on the results described above. The electrochemical data showed that the O₂ release of **1a** proceeds via successive electron oxidations from the peroxide moiety and Co(III) to Co(IV), similarly to that of 2-syn and 2-anti. 10 Water oxidation after the O2 release of 1a may proceed in a 4e⁻/2H⁺ PCET of [Co^{III}-OH]₂, assignable to intermediate B, where the 2e⁻/2H⁺ PCET of [Co^{III}- $OH]_2$ to form $[CO^{III}-O^*]_2$, O-O bond formation of $[CO^{III}-O^*]_2$, and 2e oxidation of the resultant peroxo complex successively occur (Scheme 1). As previously reported, the syn-μ-oxodioxodiiron(iv) of 6-hpa ligand forms an O-O bond, and DFT studies revealed that this O-O bond formation is energetically more favourable than the syn-to-anti transformation of the syn-dioxo form. 13 Thus, the syn form of $[Co^{III}-O^{\bullet}]_2$, fixed by the 6-hpa ligand, facilitates the O-O bond formation. This is the reason that the 6-hpa complex enhances water oxidation. The O2 evolution in the CPE at 1.4 V is less likely to be affected by the difference in redox potentials of 1.32 and 1.34 V in water oxidation by 1a and by the mixture of 2-syn and 2-anti, respectively. Thus, the most important feature in the enhancement of catalytic activity by 1a is structural control by the 6-hpa ligand, fixing the syn form of [Co^{III}-O^{*}]₂ to facilitate O-O bond formation.

The apparent catalytic rate constant (TOF s⁻¹) of 1a in the OER at pH 8.0 was estimated to be 430 s⁻¹ using the plateau-



Scheme 1 Proposed mechanism for O₂-evolution by 1a

ing current in the CVs (Fig. S10†), according to the literature. 17 The plot is shown in Fig. S11.† This value is relatively large in water oxidation catalysts, 4b though smaller than the 1900 s-1 of Masaoka's pentairon complex.6b

In this study, we synthesized and structurally characterized a new μ-OH-μ-O₂-Co(III)₂ complex with 6-hpa ligand [Co(μ-OH) $(\mu-O_2)(6-hpa)X_3$ (X = ClO₄ (1a) and PF₆ (1b)) and found that the 6-hpa ligand enhances the catalytic activity of the Co complex in the O₂ evolution by water oxidation, by structurally controlling and fixing the syn configuration.

Conflicts of interest

There are no conflicts to declare.

Data availability

The data supporting this article have been included as part of the ESI.†

References

- 1 D. Welsby, J. Price, S. Pye and P. Ekins, Nature, 2021, 597, 230-234.
- 2 (a) P. Joliot, G. Barbieri and R. Chabaud, Photochem. Photobiol., 1969, 10, 309-329; (b) B. Kok, B. Forbush and M. Mcgloin, Photochem. Photobiol., 1970, 11, 457-475; (c) A. Zouni, H.-T. Witt, J. Kern, P. Fromme, N. Krauss, W. Saenger and P. Orth, Nature, 2001, 409, 739-743; (d) Y. Umena, K. Kawakami, J. R. Shen and N. Kamiya, Nature, 2011, 473, 55-60.
- 3 S. W. Gersten, G. J. Samuels, T. J. Meyer and N. Carolina, J. Am. Chem. Soc., 1982, 104, 4029-4030.
- 4 (a) M. Kondo and S. Masaoka, Acc. Chem. Res., 2020, 53, 2140-2151; (b) M. Kondo, H. Tatewaki and S. Masaoka, Chem. Soc. Rev., 2021, 50, 6790-6831.
- 5 (a) M. Calvin, Science, 1974, 184, 375-381; (b) K. J. Young, B. J. Brennan, R. Tagore and G. W. Brudvig, Acc. Chem. Res., 2015, 48, 567-574; (c) W. T. Lee, S. B. Muñoz III, D. A. Dickie and J. M. Smith, Angew. Chem., Int. Ed., 2014, 53, 9856–9859; (d) A. K. Poulsen, A. Rompel and C. J. McKenzie, Angew. Chem., Int. Ed., 2005, 44, 6916-6920.
- 6 (a) L. D. Wickramasinghe, R. Zhou, R. Zong, P. Vo, K. J. Gagnon and R. P. Thumme, J. Am. Chem. Soc., 2015, 137, 13260-13263; (b) M. Okamura, M. Kondo, R. Kuga, Y. Kurashige, T. Yanai, S. Hayami, V. K. K. Praneeth, M. Yoshida, K. Yoneda, S. Kawata and S. Masaoka, *Nature*, 530, 465-468; (c) K. G. Kottrup D. G. H. Hetterscheid, Chem. Commun., 2016, 52, 2643-2646; (d) J. L. Fillol, Z. Codolà, I. Garcia-Bosch, L. Gómez, J. J. Pla and M. Costas, Nat. Chem., 2011, 3, 807-813.
- 7 (a) P. Sharma, S. Gupta, R. Kumar, A. Charisiadis, M. Sauban, L. Velasco, A. Saini, A. Charisiadis, D. Moonshiram and A. Draksharapu, Chem. Commun.,

2024, **60**, 14846–14849; (b) T. Nakazono, R. Mitsuda, K. Hashimoto, T. Wada and H. Tamiaki, *Inorg. Chem.*, 2024, **63**, 24041–24048; (c) T. Nakazono and T. Wada, *Inorg. Chem.*, 2021, **60**, 1284–1288; (d) D. J. Wasylenko, R. D. Palmer, E. Schott and C. P. Berlinguette, *Chem. Commun.*, 2012, **48**, 2107–2109; (e) H. Y. Du, S. C. Chen, X. J. Su, L. Jiao and M. T. Zhang, *J. Am. Chem. Soc.*, 2018, **140**, 1557–1565; (f) D. K. Dogutan, R. McGuire and D. G. Nocera, *J. Am. Chem. Soc.*, 2011, **133**, 9178–9180; (g) D. Wang and J. T. Groves, *Proc. Natl. Acad. Sci. U. S. A.*, 2013, **110**, 15579–15584.

Communication

- 8 H.-Y. Wang, E. Mijangos, S. Ott and A. Thapper, *Angew. Chem.*, *Int. Ed.*, 2014, 53, 14499–14502.
- 9 J.-W. Wang, P. Sahoo and T.-B. Lu, ACS Catal., 2016, 6, 5062–5068.
- 10 (a) T. Ishizuka, A. Watanabe, H. Kotani, D. Hong, K. Satonaka, T. Wada, Y. Shiota, K. Yoshizawa, K. Ohara, K. Yamaguchi, S. Kato, S. Fukuzumi and T. Kojima, *Inorg. Chem.*, 2016, 55, 1154–1164; (b) H. Kotani, D. Hong, K. Satonaka, T. Ishizuka and T. Kojima, *Inorg. Chem.*, 2019, 58, 3676–3682.
- 11 M. Kodera, M. Itoh, K. Kano, T. Funabiki and M. A. Reglier, *Angew. Chem., Int. Ed.*, 2005, **44**, 7104–7106.
- 12 (a) T. Tsuji, A. A. Zaoputra, Y. Hitomi, K. Mieda, T. Ogura, Y. Shiota, K. Yoshizawa, H. Sato and M. Kodera, *Angew. Chem., Int. Ed.*, 2017, **56**, 7779–7782; (b) H. Takahashi,

- K. Wada, K. Tanaka, K. Fujikawa, Y. Hitomi, T. Endo and M. Kodera, *Bull. Chem. Soc. Jpn.*, 2022, **95**, 1148–1155.
- (a) M. Kodera, Y. Kawahara, Y. Hitomi, T. Nomura, T. Ogura and Y. Kobayashi, J. Am. Chem. Soc., 2012, 134, 13236–13239;
 (b) M. Kodera, S. Ishiga, T. Tsuji, K. Sakurai, Y. Hitomi, Y. Shiota, P. K. Sajith, K. Yoshizawa, K. Mieda and T. Ogura, Chem. Eur. J., 2016, 22, 5924–5936.
- 14 (a) H. T. K. Britton and R. A. Robinson, J. Chem. Soc., 1931, 1456–1462; (b) R. Wang, J. G. Vos, R. H. Schmehl and R. Hage, J. Am. Chem. Soc., 1992, 114, 1964–1970.
- 15 The difference in O–O bond distance 0.039 Å between **1b** and **2-anti** is larger than $3\sigma = 0.012$ and 0.027 Å in **1b** and **2-anti**, respectively. The differences in Co–O–O–Co dihedral angles 7.8° and 10.0° between **1b** and **2-syn**, and **1b** and **2-anti** are much larger than $3\sigma = 0.9^\circ$, 1.2°, 1.8° in **1b**, 2-syn, **2-anti**, respectively. The difference in average Co–O_{peroxide} bond distance 0.023 Å between **1b** and **2-anti** is larger than $3\sigma = 0.09$ Å in **1b** and close to 0.024 Å in **2-anti**. These differences are meaningful.
- 16 Mean plane distances of Co, Co, O, O in the Co-O-O-Co of 1b, 0.111, 0.110, 0.281, 0.282 Å, are significantly smaller than 0.121, 0.125, 0.329, 0.325 Å of 2-syn and 0.122, 0.124, 0.340, 0.338 Å of 2-anti.
- 17 C. Costentin, S. Drouet, M. Robert and J.-M. Savéant, *Science*, 2012, 338, 90–94.